

Identification of Seawater Intrusion Distribution Patterns Using 2D Electrical Resistivity Tomography (ERT) Data in Semarang, Indonesia

Eko Minarto^{1*}, Amanda Rizky Utami¹, Lina Handayani², Yayat Sudrajat²

¹Physics Department, Faculty of Science and Analytica Data, Institute of Technology Sepuluh Nopember, Indonesia

²Geotechnology Research Center, The Indonesian Academy of Sciences

Corresponding Authors E-mail: minarto@physics.its.ac.id

Article Info

Article info:

Received: 11-01-2025

Revised: 18-05-2025

Accepted: 20-05-2025

Keywords:

Subsidence; tidal flooding; geoelectric; apparent resistivity; inversion

How To Cite:

E. Minarto, A. R. Utami, L. Handayani, and Y. Sudrajat, "Identification of Seawater Intrusion Distribution Patterns Using 2D Electrical Resistivity Tomography (Ert) Data in Semarang, Indonesia", *Indonesian Physical Review*, vol. 8, no.2, p 519-529, 2025.

DOI:

<https://doi.org/10.29303/ipr.v8i2.461>

Abstract

Various environmental problems exist in the northern coast area of Semarang, Indonesia, including land subsidence, tidal flooding, increased chloride content in several monitoring wells, and salinity in resident wells. These issues indicate a decrease in groundwater quality caused by seawater intrusion. Sanitary and health issues have a significant impact on many environmental issues, including decreased soil fertility and building damage. The problem of seawater intrusion can be identified by the geoelectric resistivity method (multi-electrode dipole-dipole configuration). The aim of this research is to detect the presence of seawater intrusion in groundwater zones and determine the extent of its distribution to the mainland. Data collection was carried out along the western canal flood. The data obtained distribution of subsurface apparent resistivity values. Interpretation of the 2D cross-sectional model identified as a seawater intrusion zone with low resistivity ($\rho < 3 \Omega m$) ranging from 0-2.600 m. Thick in the northward with a depth of 30-60 m and becomes thin in the south at 2.600 m. At a trajectory 2.600-7.000 m low resistivity is still found in a local spot. The result of the 2D cross-section model inversion shows very good result. Predicted data is quite close to the observed data shown by an average small RMS 2.37% - 4.11%. And shown by a fast convergence curve. The coastal area of Semarang is also found to be made up of five layers: alluvial soft clay, silt clay, sandy clay, granule sand, and coarse sand. These results fit with the well log data around the research area. Estimates of the distribution of seawater intrusion in more detail to the mainland need to be further investigated using other geophysical methods and testing of monitoring wells or resident wells around the research area for more accurate results.



Copyright (c) 2025 by Author(s), This work is licensed under a Creative Commons Attribution-ShareAlike 4.0 International License.

Introduction

Semarang is Central Java's capital city and the center of an industrial district on the north shore of the Java Sea (Figure 1a). It has 373.7 km² area with 1.815.729 populations in June 2018 (Population and Civil Registration Agency of Semarang). The enormous population and industrial expansion in Semarang causes the demand of ground water to continue to increase [1]. The need for ground water of Semarang residents reaches 170 thousand m³ per day or around 61.7 million m³ per year (Municipal Waterworks Semarang, 2010). Most

of this are resolved by taking groundwater through pumping in free aquifers and depressed aquifers [2]. Large-scale exploitation of groundwater can disrupt hydrogeological balance, especially in areas close to the coast [3]. The discharge of aquifers owing to groundwater absorption can cause the passage of sea water into the mainland, resulting in seawater intrusion [4] (Figure 1b).

Sea water intrusion leads in a decrease the quality of ground water [5], which has a wide-ranging influence on many elements of life, including health issues, reduced soil fertility, construction damage, and so on [6]. Indications of the occur sea water intrusion in Semarang can be seen from several environmental problems [7] that have arisen over the past few years such as tidal flooding, land subsidence, sea level rise, resident wells and observation wells that become brackish or salty, and an increase in the level of chloride in some monitoring wells [8].

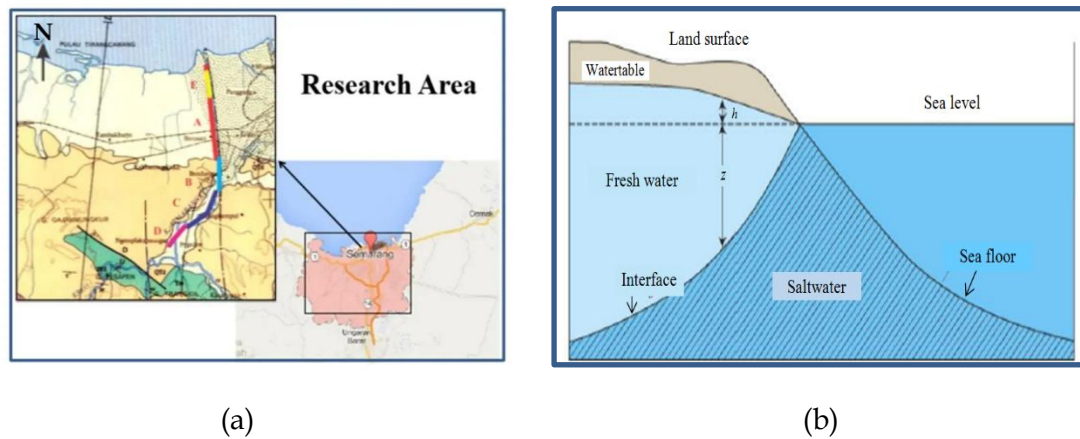


Figure 1. Research location map (Semarang) (a), and sea water intrusion mechanism (b)

The geology of the northern Semarang is dominated by quarter-age alluvial deposits [9] (Figure 2). Alluvium deposits of beaches, rivers, and lakes are found along the Semarang coast, according to the geological map [10]. The clay, silt, and sand combinations that make up these coastal alluvium deposits [11] and characterized by the repetition of silt clay which are quite dominant with fine to coarse sand inserts [12]. With several estuaries and streams, the coastal alluvium region is quite low, resembling a basin, and the water will rise in the event of a tide [13]. Seawater flows easily inland due to the lithology of alluvium deposits, which range from gravel to clay [14].

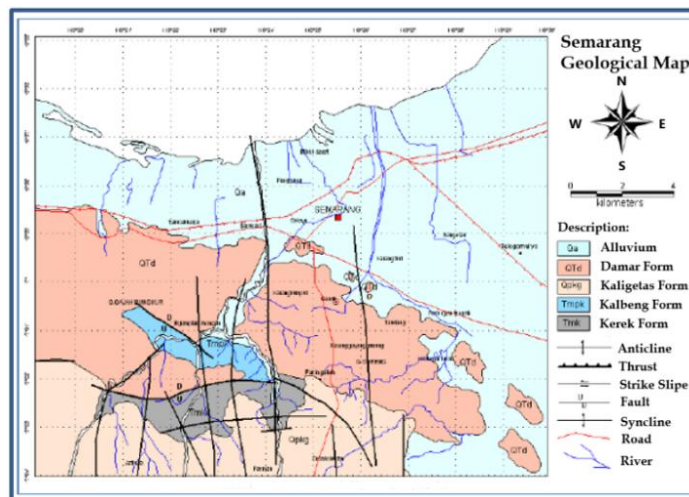


Figure 2. Geological map of Semarang [15].

Based on these problems, it is necessary to conduct research on the extent of the distribution of sea water intrusion in the coastal of Semarang. The study was conducted with a multi-electrode dipole-dipole configuration type resistivity method.

Experimental Method

There are 3 stages of processing, the first is GPS data processing serves for the analysis of the measurement trajectory location. The second step is a terrain data processing to provide topographic factors in processed data. And the third is geoelectric data processing to obtain 2D of subsurface images [16].

One of the most popular geophysical exploration techniques for a variety of geophysical investigations is geoelectric [17]. The resistivity geoelectric method is one type of geoelectric approach. Many different geophysical surveys employ the resistivity geoelectric approach because it is inexpensive and produces reliable findings [18]. It operates according to the electrical characteristics of the rocks that comprise the crust of the earth. By measuring the soil's surface, the resistivity geoelectric survey seeks to ascertain the distribution of subsurface resistance. The idea is to provide an electric current to the earth and then use two potential electrodes to monitor the potential changes (Figure 3).

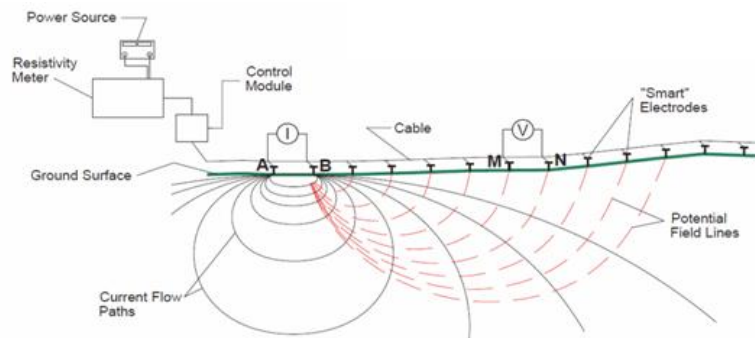


Figure 3. The basic principle of resistivity geoelectric method

The dipole-dipole configuration is commonly used in geoelectric resistivity surveys. Dipole-dipole is one of the configurations in geoelectric resistivity that is commonly used in geophysical exploration. Combining profiling and sounding techniques, so this configuration has good sensitivity for vertical and horizontal [19]. Configuring dipole-dipole multi-electrode has advantages in terms of measurement time efficiency and obtained more data. Maintain the same distance between the current and potential electrodes as "n," and the same distance between the electrodes as "a" (**Figure 4**). To enhance the depth of study, the 'n' factor rises from 1 to roughly 6 while the 'a' size remains constant [20]. The relationship between potential difference and resistivity can be expressed in the following equation:

$$\rho = k \frac{\Delta V}{I} = \frac{2\pi}{\left[\left(\frac{1}{r_1} - \frac{1}{r_2}\right) - \left(\frac{1}{r_3} - \frac{1}{r_4}\right)\right]} \frac{\Delta V}{I} \quad (1)$$

$$k = 2\pi \left[\left(\frac{1}{r_1} - \frac{1}{r_2}\right) - \left(\frac{1}{r_3} - \frac{1}{r_4}\right) \right]^{-1} = \pi a n (n+2)(n+1) \quad (2)$$

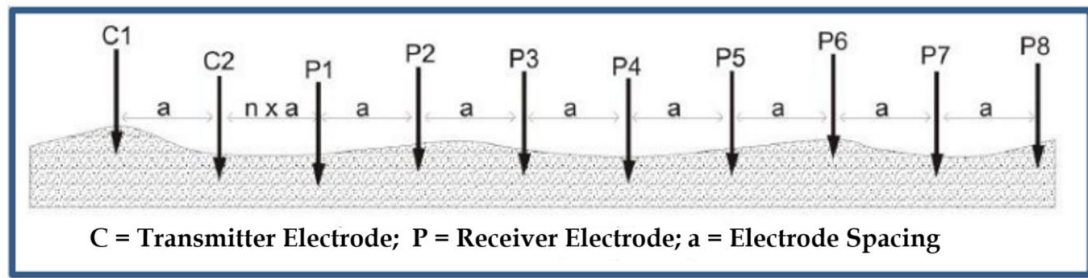


Figure 4. Dipole-dipole multielectrode configuration with 8 channel receiver electrodes [21].

Using the geoelectrical super sting model R8 / IP-56, geoelectric data is acquired (**Figure 5a**). Data acquisition along the western canal flooding by Geotechnology Research Centre Team, The Indonesian Academy of Sciences (LIPI). Data acquisition consists of 11 lines with 8 tracks with 25 m electrode spacing and 3 tracks with 10 m electrode spacing (**Figure 5b**). The selection of different electrode spacings was intended to obtain different depths penetration. The farther away from the shoreline the depth of seawater intrusion is also shallower.

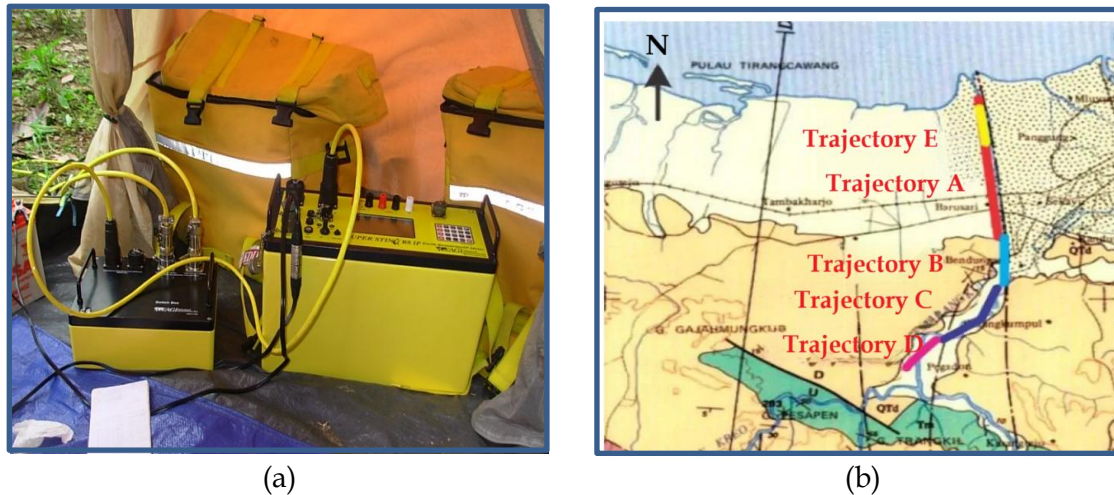


Figure 5. Geoelectrical supersting model R8 / IP-56 (a), and trajectories map (b)

Lines 1-4 consist of 56 electrodes in 1350 m length, lines 5-8 consist of 28 electrodes in 75 m length, and lines 9-11 consist of 28 electrodes in 270 m length. This trajectory is continuous and has a total length of 7 km. Furthermore, for the processing and interpretation, several interconnected trajectories are combined into one large trajectory, so that the results of 5 combined trajectories are obtained (Table 1). Trajectory A is a combination of lines 1-3, trajectory B represents line 4, trajectory C is a combination of lines 5-7, trajectory D represents line 8, and trajectory E is a combination of lines 9-11. The track has a direction perpendicular to the coastline to find out how far the distribution of seawater intrusion to the mainland.

Information on the distribution of subsurface physical attributes is obtained by the inversion process, a field data processing method that makes use of statistical and mathematical solutions [22]. Estimating the physical properties of the unknown rock is the aim of the inversion procedure. Curve fitting between the field data and the mathematical model may be used to analyze the field data during the inversion process [23]. In general, the inversion problem can be expressed by the equation:

$$d = F(m) + e \quad (3)$$

Where d is the data vector, m is the model parameter vector, e is the error vector, and F is the forward modeling function. In this research, the inversion method is used Non-Linear Conjugate Gradient (NLCCG). The NLCCG method is used to minimize the objective function which is defined as follows [24]:

$$\Psi(m) = (d - F(m))^T V^{-1} (d - F(m)) + \lambda m^T L^T L m \frac{\Delta V}{I} \quad (4)$$

Where λ is the regulation parameter in the form of a positive number, V is the matrix that regulates the variation of the error e , and L is the operator matrix. The NLCCG algorithm uses the Polak-Ribiere NLCCG variation to eliminate the equation of the objective function.

The search for a model for NLCCG is determined by determining the objective function minimization variable which is given the initial model m_0 , so that the model equation can be expressed to:

$$m_{l+1} = m_l + \alpha_l p_l \quad (5)$$

With m_{l+1} it is a new model from the initial modeling which has been added with a system that can speed up the inversion process or referred to as a preconditioner [25].

Table 1. Acquisition data line characteristic

No.	Line number	Electrode-spacing-length	Trajectory
1.	1	25 m electrode spacing, 56 electrodes in 1350 m length	Trajectory A
	2		
	3		
2.	4	25 m electrode spacing, 56 electrodes in 1350 m length	Trajectory B
3.	5	25 m electrode spacing, 28 electrodes in 75 m length	Trajectory C
	6		
	7		
4.	8	25 m electrode spacing, 28 electrodes in 75 m length	Trajectory D
5.	9	10 m electrode spacing, 28 electrodes in 270 m length	Trajectory E
	10		
	11		

Results And Discussion

The result of the 2D cross-section model inversion for each trajectory shows a very good result. Predicted data is quite close to measured data shown by small RMS and also a fast convergence curve. Figure 6 shows a cross plot of measured vs predicted apparent resistivity for trajectory A with an RMS is 3.81 % and Figure 7 shows the convergence curve of resistivity inversion at 8th iterations for trajectory A. Whereas, the measured and calculated apparent resistivity pseudo section for trajectory A shown in **Figure 8**. For trajectory B RMS is 2.64% and convergence at 4th iterations, for trajectory C RMS is 2.42 % and convergence at 5th iterations, for trajectory D RMS is 4.11 % and convergence at 7th iterations, and for trajectory E RMS is 2.37% and convergence at 5th iterations.

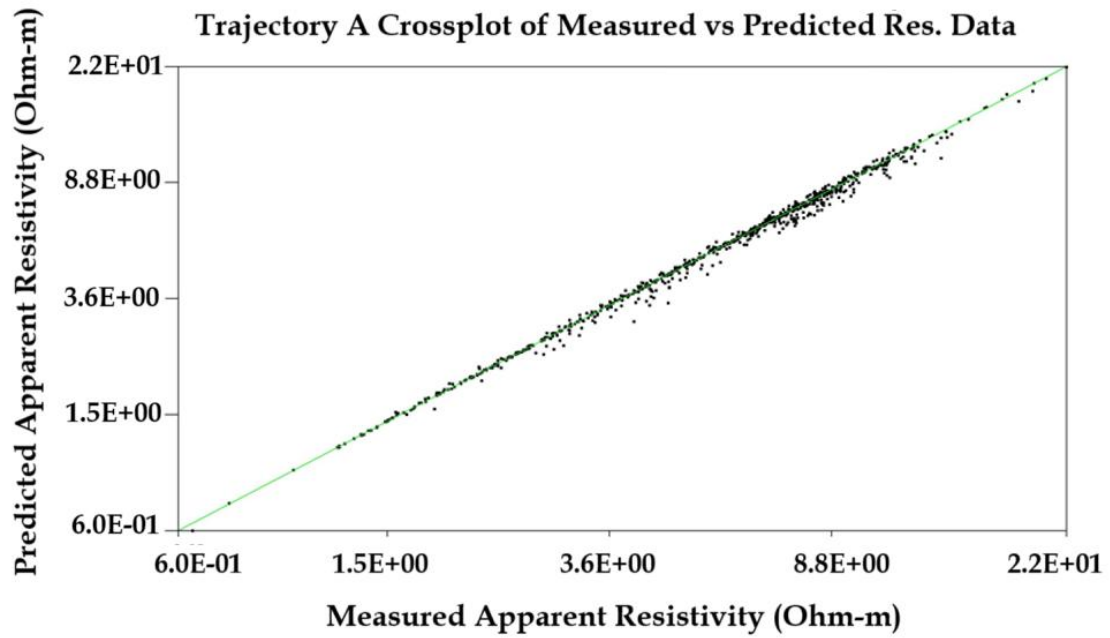


Figure 6. Cross plot of measured vs predicted apparent resistivity

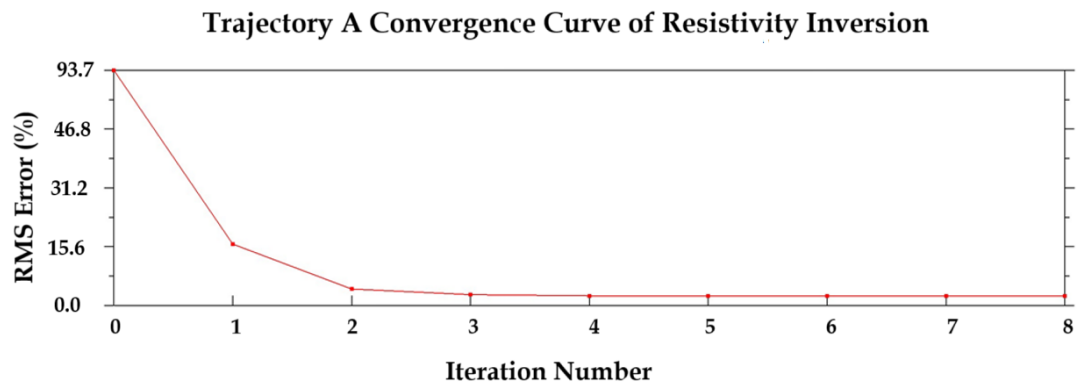


Figure 7. Convergence curve of resistivity inversion

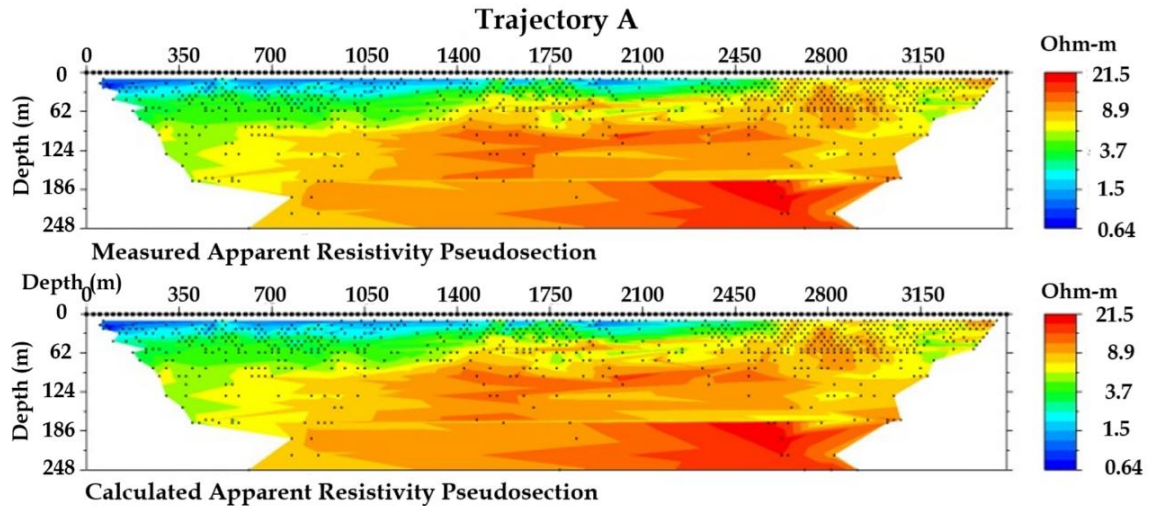


Figure 8. Measured and calculated apparent resistivity pseudo section

The subsurface resistivity value distribution for trajectory A is displayed in Figure 9. The very low resistivity value $\rho \leq 3 \Omega\text{m}$ is evenly distributed at the top from points 0 to 2.600 m with a depth of 30-60 m, estimated as a soft clay layer. The soft clay layer has very small granules and an impermeable layer, so the fluid will be retained and trapped in this layer. It is suspected that the fluid that fills this layer is seawater.

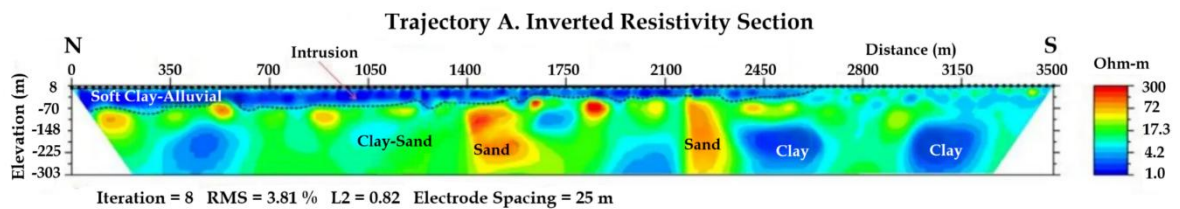


Figure 9. 2D cross-section model inversion for trajectory A

Figure 10 and Figure 11 show the distribution of subsurface resistivity values for trajectory B and trajectory C. The very low resistivity value $\rho \leq 3 \Omega\text{m}$ at 2.600-7.000 m is still found in a local spot. This layer is estimated as a soft clay layer with very small granules and impermeable suspected thought to contain seawater. The result of the 2D cross-section model inversion shows very good result. Predicted data quite close with observed data shown by average small RMS 2.42% - 2.64%. And shown by a fast convergence curve.

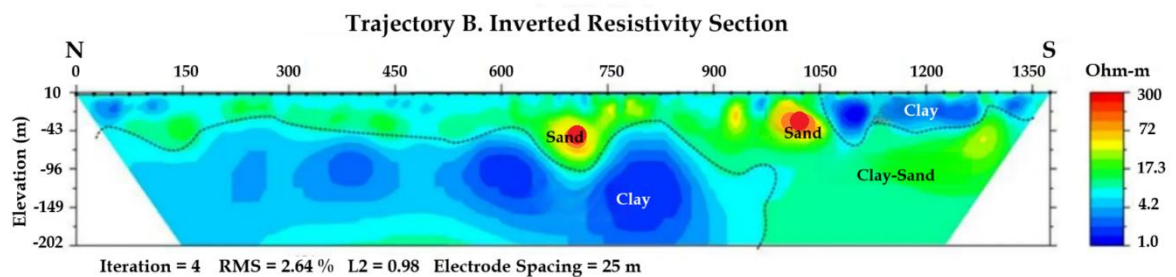


Figure 10. 2D cross-section model inversion for trajectory B

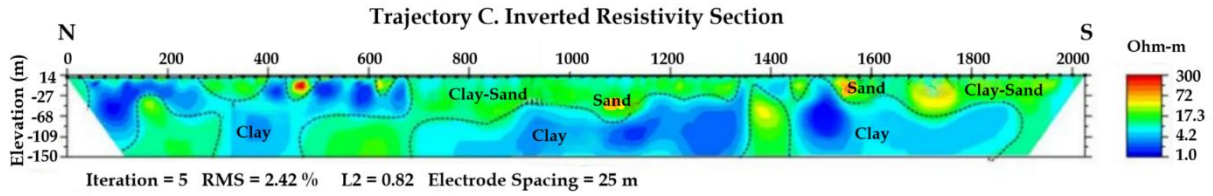


Figure 11. 2D cross-section model inversion for trajectory C

Figure 12 shows the distribution of subsurface resistivity values for trajectory D. The very low resistivity value $\rho \leq 3 \Omega\text{m}$ is still found in a few local spots although very rare and shallow. Due to having furthest from the coastline. The result of the 2D cross-section model inversion for trajectory D shows very good result. Predicted data quite close with observed data shown by a small RMS 4.11%. And shown by a fast convergence curve at 7th iterations.

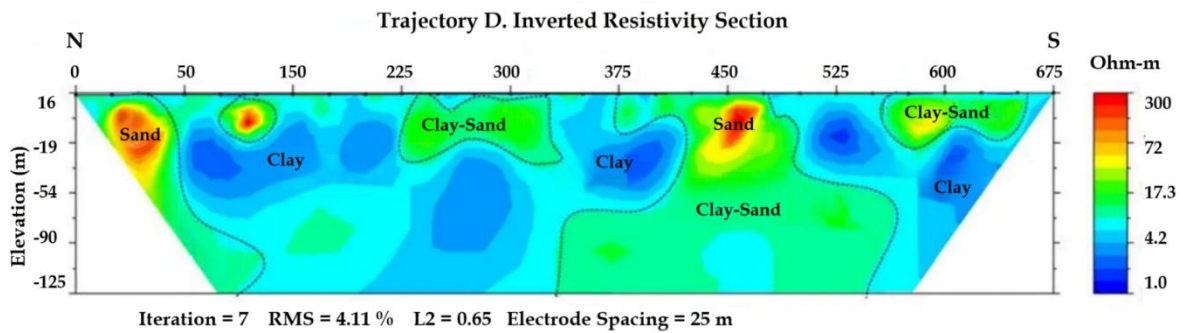


Figure 12. 2D cross-section model inversion for trajectory D

Figure 13 shows the distribution of subsurface resistivity values for trajectory E. The very low resistivity value $\rho \leq 3 \Omega\text{m}$ is evenly distributed at the top with a depth of 30 m estimated as a soft clay layer suspected thought to contain seawater. The result of the 2D cross-section model inversion shows very good result. Predicted data quite close with observed data shown by small RMS 2.37% at 5th iterations.

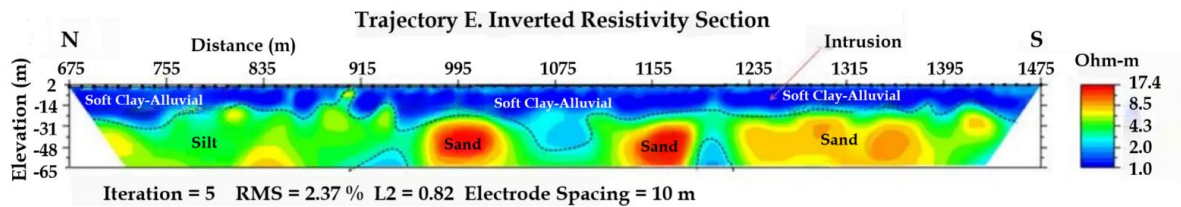


Figure 13. 2D cross-section model inversion for trajectory E

Table 2 shows lithological interpretation from the 2D cross-section model inversion result that Semarang coastal is composed of 5 layers: Alluvial soft clay, silt clay, sandy clay, granules sand, and coarse sand. This result fits with the well log data around research area (Table 3).

Table 2. lithological interpretation from the 2D cross-section model inversion result.






Color	Resistivity	Lithology	Interpretation
	$\rho \leq 3 \Omega\text{m}$	Alluvial soft clay	Sea water intrusion
	$3 \Omega\text{m} \leq \rho \leq 8.5 \Omega\text{m}$	Silt clay	Sea water intrusion
	$8.5 \Omega\text{m} \leq \rho \leq 50 \Omega\text{m}$	Sandy clay	Salty
	$50 \Omega\text{m} \leq \rho \leq 100 \Omega\text{m}$	Granules sand	Fresh/tasteless
	$100 \Omega\text{m} \leq \rho \leq 300 \Omega\text{m}$	Coarse sand	Fresh/tasteless

Table 3. Madukoro Well log lithological data.

Layer	Depth
Alluvial soil	0-2 m
Clay	2-30 m
Sand-Silt	30-45 m
Clay	45-65 m
Silt	65-80 m
Sand	80-110 m

Conclusion

This study resulted that the interpretation of the 2D cross-section model identified as a seawater intrusion zone that has a low resistivity value of less than 3 ohm.m ($\rho < 3 \Omega\text{m}$) extending at 0-2.600 m. Thick in the northward with a depth of 30-60 m and becomes thin in the south at 2.600 m. At a trajectory 2.600-7.000 m low resistivity are still found in a local spot. The result of the 2D cross-section model inversion shows very good result. Predicted data quite close with observed data shown by average small RMS 2.37% - 4.11%. And shown by a fast convergence curve. Also obtained that the area of Semarang coastal is composed of 5 layers: Alluvial soft clay, silt clay, sandy clay, granules sand, and coarse sand. This result fits with the well log data around the research area. The results of this study can be used as a reference for how deep and how far seawater intrusion goes into the land. Of course, this result can be used by the local government as a warning for residents to make daily consumption wells. Estimates of the distribution of seawater intrusion in more detail to the mainland need to be further investigated using other

geophysical methods and testing of monitoring wells or resident wells around the research area for more accurate results.

Acknowledgments

No funding was received to assist with the preparation of this manuscript. I would like to thank to Geotechnology Research Center, The Indonesian Academy of Sciences (Geoteknologi LIPI) for kindly provided the data in this research.

References

- [1] W. Lo, S. N. Purnomo, D. Sarah, S. Aghnia, and P. Hardini, "Groundwater Modelling in Urban Development to Achieve Sustainability of Groundwater Resources: A Case Study of Semarang City, Indonesia," *Water*, vol. 13, no. 10, p. 1395, May 2021.
- [2] S. Widada, B. Rochaddi, C. A. Suryono, and I. Irwani, "Intrusi Air Laut di Pesisir Tugu Kota Semarang Berdasarkan Resistiviti dan Hidrokimia," *J. Kel. Trop.*, vol. 21, no. 2, p. 75, Dec. 2018.
- [3] M. Perumal, S. Sekar, and P. C. S. Carvalho, "Global Investigations of Seawater Intrusion (SWI) in Coastal Groundwaters in the Last Two Decades (2000–2020): A Bibliometric Analysis," *Sustainability*, vol. 16, no. 3, p. 1266, Feb. 2024.
- [4] N. Alfarrak and K. Walraevens, "Groundwater Overexploitation and Seawater Intrusion in Coastal Areas of Arid and Semi-Arid Regions," *Water*, vol. 10, no. 2, p. 143, Feb. 2018.
- [5] S. Das, P. K. Maity, and R. Das, "Remedial Measures for Saline Water Ingression in Coastal Aquifers of South West Bengal in India," *MOJES*, vol. 3, no. 1, Jan. 2018.
- [6] J. Mas-Pla, G. Ghiglieri, and G. Uras, "Seawater intrusion and coastal groundwater resources management. Examples from two Mediterranean regions: Catalonia and Sardinia," *Contributions to Science*, no. 10, pp. 171–184, 2014.
- [7] S. Badaruddin, A. D. Werner, and L. K. Morgan, "Characteristics of active seawater intrusion," *Journal of Hydrology*, vol. 551, pp. 632–647, Aug. 2017.
- [8] I. R. Suhelmi and H. Prihatno, "Model Spasial Dinamik Genangan Akibat Kenaikan Muka Air Laut Di Pesisir Semarang (Spatial Dynamic Model of Inundated area due to Sea Level rise at Semarang coastal Area)," *Jurnal Manusia dan Lingkungan*, vol. 21, no. 1, Art. no. 1, May 2014.
- [9] D. Sarah, L. M. Hutasoit, R. M. Delinom, and I. A. Sadisun, "Natural Compaction of Semarang-Demak Alluvial Plain and Its Relationship to the Present Land Subsidence," *Indonesian J. Geosci.*, vol. 7, no. 3, pp. 273–289, Oct. 2020.
- [10] D. D. Wardhana, H. Harjono, and S. Sudaryanto, "Struktur Bawah Permukaan Kota Semarang Berdasarkan Data Gayabarat," *Riset Geologi dan Pertambangan - Geology and Mining Research*, vol. 24, no. 1, Art. no. 1, May 2014.
- [11] B. Rochaddi and I. Pratikto, "Deliniasi Batas Biogeofisik Wilayah Daratan Pesisir," *ILMU KELAUTAN: Indonesian Journal of Marine Sciences*, vol. 11, no. 1, pp. 23–30, 2006.
- [12] S. Khumaedi, "Geophysical And Hydrochemical Approach For Seawater Intrusion In North Semarang, Central Java, Indonesia," *Geomate*, vol. 12, no. 31, Mar. 2017.
- [13] A. T. Ahmed and B. Askri, "Seawater Intrusion Impacts on the Water Quality of the Groundwater on the Northwest Coast of Oman," *Water Environment Research*, vol. 88, no. 8, pp. 732–740, 2016.
- [14] A. Yuliyanti, D. Sarah, and E. Soebowo, "Pengaruh Lempung Ekspansif Terhadap Potensi Amblesan Tanah Di Daerah Semarang," *J.Ris.Geo.Tam*, vol. 22, no. 2, p. 91, Nov. 2012.

- [15] R. E. Thanden, "Peta geologi lembar Magelang dan Semarang, Jawa : Geological map of the Magelang and Semarang sheets, Jawa."
- [16] S. Sankaran, S. Sonkamble, K. Krishnakumar, and N. C. Mondal, "Integrated approach for demarcating subsurface pollution and saline water intrusion zones in SIPCOT area: a case study from Cuddalore in Southern India," *Environ Monit Assess*, vol. 184, no. 8, pp. 5121–5138, Aug. 2012.
- [17] E. A. Arliska, P. Anda, and E. S. Hasan, "Identifikasi Intrusi Air Laut Menggunakan Metode Vertical Electrical Sounding Di Kecamatan Sawa," *JGE*, vol. 8, no. 3, pp. 197–209, Nov. 2022.
- [18] D. Panjaitan, J. Tarigan, A. Rauf, and E. S. Nababan, "Determining sea water intrusion in shallow aquifer using Chloride Bicarbonate Ratio Method," *IOP Conf. Ser.: Earth Environ. Sci.*, vol. 205, p. 012029, Dec. 2018.
- [19] A. P. Aizebeokhai, "Geoelectrical Resistivity Imaging in Environmental Studies," in *Appropriate Technologies for Environmental Protection in the Developing World*, E. K. Yanful, Ed., Dordrecht: Springer Netherlands, pp. 297–305, 2009.
- [20] Y.-C. Hung, H. Wang, P.-L. Wu, H.-C. Liu, and C.-P. Lin, "3D Effect and countermeasure of 2D geoelectrical imaging of a subsurface linear structure," *Engineering Geology*, vol. 338, p. 107603, Aug. 2024.
- [21] F. Stumm and M. Como, "Delineation of Salt Water Intrusion through Use of Electromagnetic-Induction Logging: A Case Study in Southern Manhattan Island, New York," *Water*, vol. 9, no. 9, p. 631, Aug. 2017.
- [22] P.-S. Huang and Y.-C. Chiu, "A Simulation-Optimization Model for Seawater Intrusion Management at Pingtung Coastal Area, Taiwan," *Water*, vol. 10, no. 3, p. 251, Feb. 2018.
- [23] S. Widada, A. Satriadi, and B. Rochaddi, "Kajian Potensi Air Tanah Berdasarkan Data Geolistrik Resistiviti Untuk Antisipasi Kekeringan Di Wilayah Pesisir Kangkung, Kabupaten Kendal, Privinsi Jawa Tengah," *J. Kel. Trop.*, vol. 20, no. 1, p. 35, Jul. 2017.
- [24] W. Rodi and R. L. Mackie, "Nonlinear conjugate gradients algorithm for 2-D magnetotelluric inversion," *GEOPHYSICS*, vol. 66, no. 1, pp. 174–187, Jan. 2001.
- [25] Z. Xu, B. X. Hu, and M. Ye, "Numerical modeling and sensitivity analysis of seawater intrusion in a dual-permeability coastal karst aquifer with conduit networks," *Hydrol. Earth Syst. Sci.*, vol. 22, no. 1, pp. 221–239, Jan. 2018.